Remote Sensing of Environment 114 (2010) 2853–2862

Contents lists available at ScienceDirect

Remote Sensing of Environment

journal homepage: www.elsevier.com/locate/rse

Interpretation of Aura satellite observations of CO and aerosol index related to the December 2006 Australia fires

Mingzhao Luo [a], Christopher Boxe [a,*], Jonathan Jiang [a], Ray Nassar [b,c], Nathaniel Livesey [a]

[a] Earth and Space Science Division, Jet Propulsion Laboratory, California Institute of Technology, Pasadena, CA 91109, USA
[b] Centre for Global Change Science, Department of Physics, University of Toronto, Toronto, Canada ON M5S 1A7
[c] Centre for Global Change Science, Department of Geography, University of Toronto, Toronto, Canada ON M5S 1A7

ARTICLE INFO

Article history:
Received 3 April 2010
Received in revised form 7 July 2010
Accepted 17 July 2010

Keywords:
Remote sensing
Satellite observations
TES
OMI
MLS
GEOS-Chem
HYSPLIT

ABSTRACT

Enhanced carbon monoxide (CO) in the upper troposphere (UT) is shown by nearly collocated Tropospheric Emission Spectrometer (TES) and Microwave Limb Sounder (MLS) measurements near and down-wind from the known wildfire region of SE Australia from December 12th–19th, 2006. Enhanced ultraviolet (UV) aerosol index (AI) derived from the Ozone Monitoring Instrument (OMI) measurements correlates with these high CO concentrations. The Hybrid Single Particle Langrangian Integrated Trajectory (HYSPLIT) model back trajectories trace selected air parcels, where TES observes enhanced CO in the upper and lower troposphere, to the SE Australia fire region as their initial location. Simultaneously, they show a lack of vertical advection along their tracks. TES retrieved CO vertical profiles in the higher and lower southern latitudes are examined together with the averaging kernels and show that TES CO retrievals are most sensitive at approximately 300–400 hPa. The enhanced CO observed by TES in the upper (215 hPa) and lower (681 hPa) troposphere are, therefore, influenced by mid-tropospheric CO. GEOS-Chem model simulations with an 8-day emission inventory, as the wildfire source over Australia, are sampled to the TES/MLS observation times and locations. These simulations only show CO enhancements in the lower troposphere near and down-wind from the wildfire region of SE Australia with drastic underestimates of UT CO plumes. Although CloudSat along-track ice-water content curtains are examined to see whether possible vertical convection events can explain the high UT CO values, sparse observations of collocated Aura CO and CloudSat along-track ice-water content measurements for the single event precludes any conclusive correlation. Vertical convection that uplifts the fire-induced CO (*i.e.*, most notably referred to as pyro-cumulonimbus (pyroCb)) may provide an explanation for the incongruence between these simulations and the TES/MLS observations of enhanced CO in the UT.

1. Introduction

Apart from being devastating to local ecosystems and economies, biomass burning and wildfires significantly alter air quality on regional to hemispheric scales (van der Werf et al., 2006) and are an important component of the climate system. They are now recognized to be a major contributor to the global emissions of trace gases and aerosols, significantly affecting the atmospheric chemistry, degrading air quality, and impacting the radiative transfer in the atmosphere (*e.g.*, Seiler & Crutzen, 1980; Logan et al., 1981; Crutzen & Andrea, 1990; Liousse et al., 1996; Andrea & Merlet, 2001). One of the principal trace gas species produced during biomass burning events is carbon monoxide (CO). CO plays a central role in the atmospheric chemistry by acting as a major sink for hydroxyl radicals (•OH) and through its role in the production of ozone (O_3). It is produced as a result of an incomplete combustion and the oxidation of methane and non-methane hydrocarbons (NMHCs) and is principally removed by a reaction with OH. CO is a major ozone precursor, and it also contributes to climate change through its effect on ozone and methane chemistry (West et al., 2009a,b). With biomass burning and oxidation of naturally occurring volatile hydrocarbons accounting for nearly 50% of tropospheric CO (Logan et al., 1981; Duncan et al., 2007), monitoring changes in these sources, changes in anthropogenic sources, and subsequent transports are key to assessing the impact on tropospheric chemistry and near-surface air quality. CO's relatively long lifetime (~2 months), makes it an excellent tracer of transport and source variability (Badr & Probert, 1994). The increase in global tropospheric CO from 1970 to the late 1980s has been linked to increasing anthropogenic emissions (Khalil & Rasmussen, 1988; Yurganov et al., 1997). Subsequent studies found that global tropospheric CO abundances leveled off and began to decrease from 1990 to 2000 because of tighter controls on automobile emissions (Novelli et al., 1994; Khalil & Rasmussen, 1994; Bakwin et al., 1994; Parrish et al., 2002; Duncan et al., 2007). However, several recent studies have postulated possible large-scale increases and variations in biomass burning sources in the hot and dry rural regions due to climate change (Yurganov et al., 2004; Lapina et al., 2006; Kasischke & Tretsky, 2007; van der Werf et al., 2008; Yurganov et al., 2008).

* Corresponding author.
E-mail address: christopher.boxe@jpl.nasa.gov (C. Boxe).

0034-4257/$ – see front matter © 2010 Elsevier Inc. All rights reserved.
doi:10.1016/j.rse.2010.07.003

Although fires are devastating to ecosystems, they are also an integral part of the cycling of ecosystems, particularly over regions that experience frequent droughts (*e.g.,* Australia and South Africa). As a matter of fact, some seed plants exhibit an ecological adaptation in fire-prone regions, in which a fire triggers seed release — termed serotiny (Salvatore et al., 2010; Cowling & Lamont, 1985). This behavior is an adaptation to an environment that experiences frequent fires, and in which post-fire environments yield the best germination and seeding survival rates. Fire-prone parts of the world, for instance, contain plants that have fire-mediated serotiny, such as angiosperms, eucalyptus, erica, and conifer.

Signatures from biomass burning are some of the main features observed from space (Lamarque et al., 2003; Edwards et al., 2004; Turquety et al., 2007; McMillan et al., 2008; Yurganov et al., 2008), due to both the large CO concentrations resulting from these fires and the fact that the fire plumes are often rapidly transported toward the free troposphere, where the IR remote sensors are most sensitive. Some of these lofting events are rapid as expressed by Fromm et al. (2005, 2006), which may primarily be due to conditions of extreme convection with sufficient energy to efficiently transport a large amount of material from the planetary boundary layer to the upper troposphere–lower stratosphere (UTLS) — most notably referred to as pyro-cumulonimbus (pyroCb) eruptions. Guan et al. (2008) recently simulated pyroCb events using the NCAR Community Atmosphere Model (CAM) with a plume-rise parameterization scheme to account for CO over Africa and its export during SAFARI 2000. Their CAM simulation with the plume-rise parameterization scheme shows a substantial improvement between the modeled and aircraft-measured vertical distribution of CO over the Southern Africa biomass burning area. They also concluded that the effect of the plume-rise on free tropospheric CO is more important for the source area (*i.e.*, short-distance transport) than for remote areas (*i.e.*, long-distance transport).

Australia's dry, windy, and hot climates cause it to be prone to wildfires. Bushfires are a regular feature of the summer, and over the past 40 years more than 250 people have been killed in bushfires (http://www.alertnet.org/thenews/newsdesk/SP65484.htm). During the late Austral spring season of 2006, fires burned across many of its regions, including Western Australia, Queensland, Cape York Peninsula, New South Wales, and Victoria. Fire hotspots are routinely measured by several space-borne remote sensors, such as the Along-Track Scanning Radiometer (ATSR, Arino et al., 2007) and the MODerate resolution Imaging Spectroradiometer (MODIS, Justice et al., 2002). These instruments allow a good evaluation of the location of the main fires under satellite overpass. Other useful data that help estimate the fire plume heights includes Infrared/Visible (IR/Vis) images taken by the geostationary satellite (*e.g.,* Japanese Multi-functional Transport Satellite-1R (MTSAT-1R) satellite over Australia) and along-track curtain images of back scatter signal from the Cloud-Aerosol Lidar and Infrared Pathfinder Satellite Observation (CALIPSO). Scientists around the world formed an on-line discussion group (http://tech.groups.yahoo.com/group/pyrocb/) sharing information, data, and analyses on all major fire events. During the December 2006 Australia fire season, the group collectively identified three major pyro-convection events, Nov. 29th, December 10th and December 14th, two of which occurred in Victoria. The conclusions are mostly based on analyses of the isolated cold temperature spots shown in the MTSAT-1R satellite images.

Dirksen et al. (2009) recently investigated the December 2006 Australian forest fires using satellite observations of aerosol from the Ozone Monitoring Instrument (OMI) and the Cloud-Aerosol with Orthogonal Polarization (CALIOP), and the TM4 chemistry transport model. The intense heat from the fires presumably caused pyro-convective lofting, which injected aerosol particles into the jet stream. Dirksen et al. (2009) track the resulting aerosol plume using Aerosol Absorbing Index (AAI) observations from OMI and found that it circumnavigated the world in 12 days. Using data from both the OMI and CALIOP, they also show that the plume resided in the upper troposphere at different stages of its evolution. Constrained by OMI O_2–O_2 retrievals, the TM4 (Tracer Model version 4) chemistry transport model was able to mimic the high injection height (10 km or 250 hPa) of the aerosol plume, associated with pyro-convective lofting.

The primary goals of this study are to present the observations made by three instruments (TES, MLS and OMI) on the Aura satellite during December 11th–19th, 2006 Australia fires, to demonstrate that for certain severe fire events like these, models (*e.g.,* GEOS-Chem) need a plume-rise scheme to simulate the long-range tracer transport in the mid-troposphere, and to conclude the needs in vertical, spatial and temporal resolutions in the future satellite observations in analyzing the evolutions of fire events. First, we discuss the enhanced CO concentrations observed by the collocated TES and MLS measurements in the upper and lower troposphere and near and down-wind from the known wildfire region of Southeast (SE) Australia, where TES averaging kernels were used to assess the vertical sensitivity of the TES CO retrievals. Given that chemical tracer observations for fire events, especially with vertical measurement resolving capability, are rarely reported in the open literature (Livesey et al., 2004), the enhanced OMI aerosol index (AI) correlated with high CO concentrations, in conjunction with co-located TES/MLS CO observations, were also evaluated to identify if the chemical tracer CO and aerosol observations on the Aura platform are consistent in describing the fire plume transport events. The HYSPLIT model was used to verify the source of the measured CO concentrations away from SE Australia. Lastly, we discussed GEOS-Chem simulations of CO with 8-day Global Fire Emission Database version 2 (GFED v2) emissions as the wildfire source over Australia, which are sampled to the TES/MLS observation times and locations. From this investigation, we show that there is a need for future satellite observations and model developments to advance the knowledge on the influence of fire events on regional and global air quality and atmospheric chemistry and dynamics.

2. TES and MLS CO and OMI AI observations of Australia region in December 2006

CO observations from TES and MLS, and UV absorbing aerosol indices (AI) obtained from OMI, on the Aura satellite are examined for the Australia fire dates of December 12th–19th, 2006. TES operates in nadir-viewing mode and provides CO volume mixing ratio (VMR) vertical profiles from the surface to the upper troposphere with limited vertical resolution (Beer, 2006). MLS operates in limb-viewing mode and provides CO VMR vertical profiles at the observation tangents of a 2–3 km thick layer for ~215 hPa and above (Waters et al., 2006). OMI's AI is a measure of departures of observed UV spectra from the model spectra without aerosol loading, and its magnitude is a good indicator of the absorbing aerosol amount in the atmosphere (Torres et al., 2007).

Fig. 1 shows the spatially interpolated CO VMR fields at 215 hPa, obtained from TES and MLS data for December 16th–17th, 2006, respectively. CO data plots at the TES footprints can be found on the TES website (http://tes.jpl.nasa.gov/visualization/SCIENCE_PLOTS/TES_L3_-Daily.htm). Both instruments observe enhanced CO mixing ratios, at almost identical locations, in this upper tropospheric level. These large CO values in the tropics are associated with the vertical advection of CO generated from biomass burnings. In the high southern latitudes, the enhanced CO observed by the two instruments is associated with the intense fires (http://earthobservatory.nasa.gov/NaturalHazards/). The locations are a few hundred to a couple of thousand kilometers away from the known fire regions of SE (Victoria) Australia. The values of CO VMR are as large as 400 ppbv for TES at 215 hPa near 32°S, 170°W. The MLS CO VMR at 215 hPa are twice as compared to those of TES, but the MLS CO data are known to be positively biased by a factor of 2 (Livesey et al., 2008). Nedelec et al. (2005) has reported similar high CO values (300–800 ppbv) detected by the aircraft measurements at 8 km during the MOZAIC (Measurements of Ozone aboard Airbus in-service airCraft)

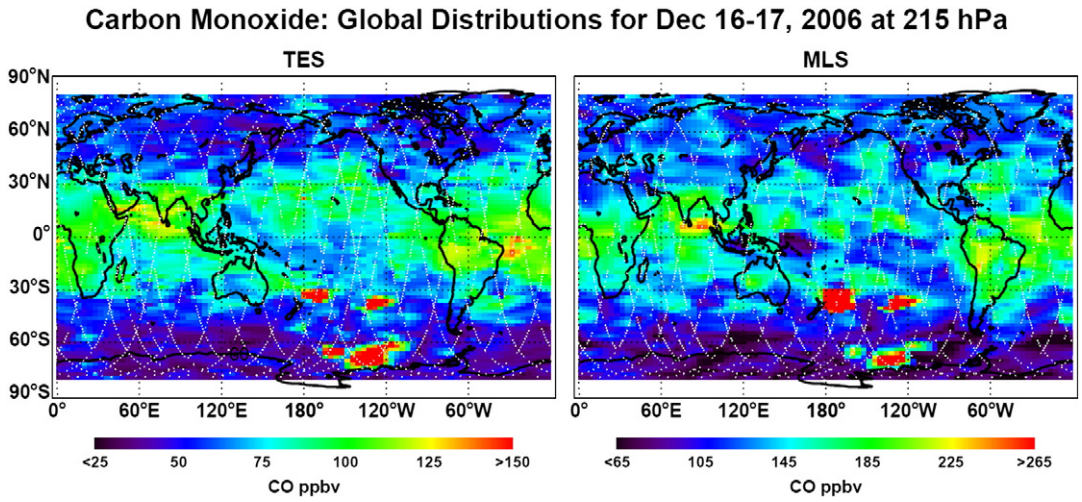

Fig. 1. Left panel: TES retrievals of CO from global survey observations taken on December 16th–17th, 2006 at 215 hPa. Right panel: MLS retrievals of CO at 215 hPa from the profiles closest to those of TES in location and time. The images are from spatially interpolated TES and MLS CO data. The white marks are TES profile geolocations or those of MLS. The high bias in MLS CO values will be corrected in the new version data (V003).

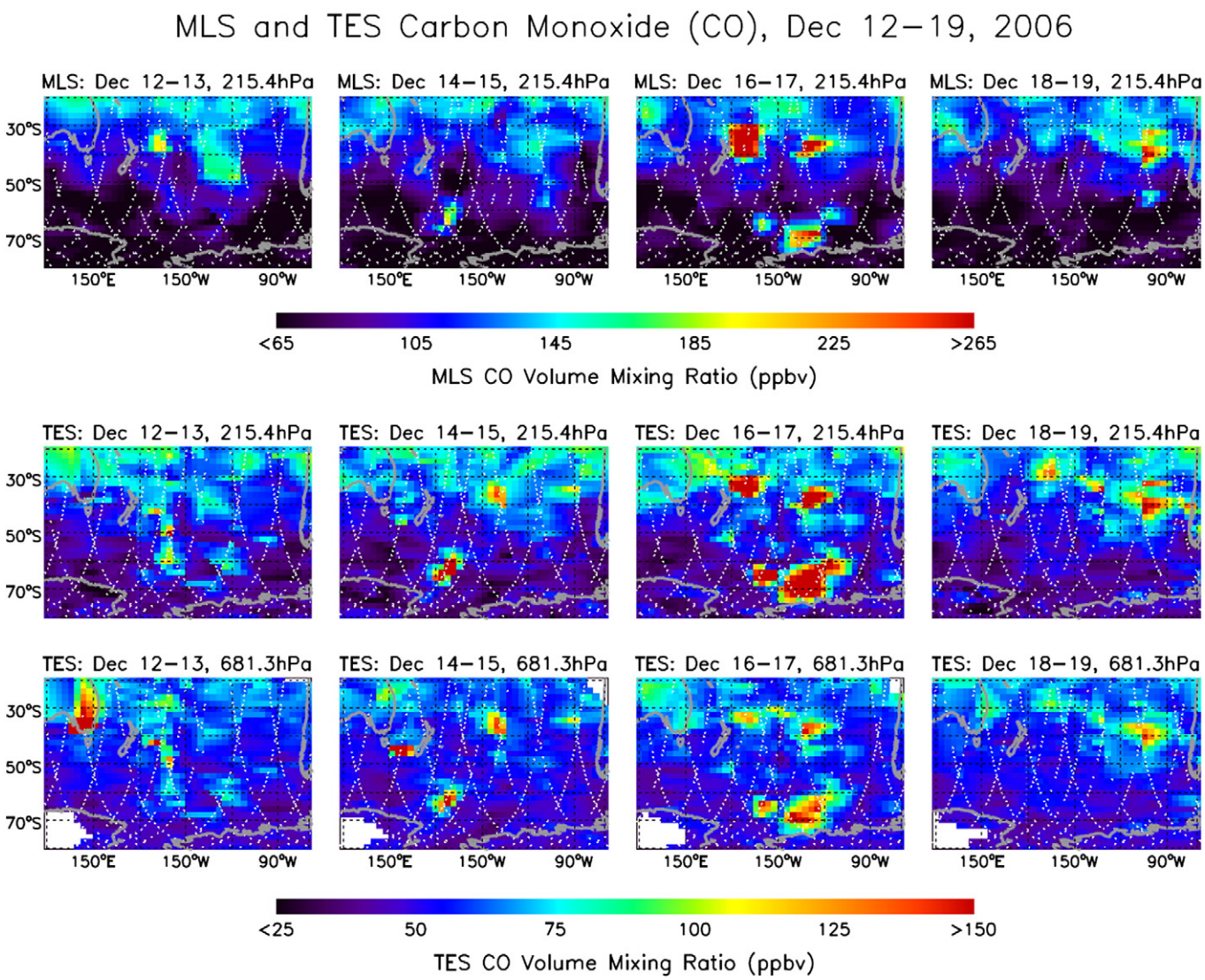

Fig. 2. Top row: MLS CO at 215 hPa (with TES observation operator applied); Mid row: TES CO at 215 hPa; Bottom row: TES CO at 681 hPa. The four columns: TES Global Surveys of December 12th–13th, December 14th–15th, December 16th–17th, and December 18th–19th, 2006. The location of the TES footprints and MLS tangent points are marked by the white symbols with the remainder of the distribution determined through spatial interpolation.

flights between Europe and East Asia spring and summer 2003 over and down-wind from the boreal forest fires around Lake Baikal.

CO data from TES at 681 hPa and 215 hPa and MLS at 215 hPa for December 12th–19th, 2006 are examined in the Australia region. Fig. 2 shows spatially interpolated TES and MLS CO VMRs. Since TES Global Survey (GS) observations along Aura orbit tracks are taken approximately every other day (26 h on, followed by 22 h off), the continually observed MLS data are selected closest to those of TES. The CO spatial distribution patterns for TES and MLS CO at 215 hPa are similar for the four GS time periods.

The TES retrieved CO profiles have limited vertical resolution that can be described by the averaging kernels and the degrees of freedom for signal (DOFS). For the two latitude bands of the Australia region, 27°S–43°S and 49°S–72°S, Fig. 3 shows the mean averaging kernels for the TES CO profiles with CO > 120 ppbv. The DOFSs for the two latitude bands are 1.4 and 1.0, respectively. As described by Rodgers (2000) and Luo et al. (2007), the retrieved CO profile is the combination of the true CO profile, vertically smoothed by the averaging kernel and the contribution from the a priori profile. For the latitude band between 49°S and 72°S (see Fig. 3, right panel), the TES CO retrievals are largely sensitive to 400–250 hPa, and the TES CO retrieved values at 215 and 618 hPa are, therefore, both influenced heavily by the true CO values at 400–250 hPa and the a priori values at all levels. We cannot conclude that the true CO values in the lower troposphere (681 hPa, bottom row in Fig. 2) far away from the source region of SE Australia are enhanced.

The TES operators are applied to the vertical profiles of the MLS CO retrievals shown in Fig. 2, top row (Osterman et al., 2009). This process treats MLS CO profiles as the 'truth' and simulates the profile that TES would have retrieved for the same air sampled by MLS with TES averaging kernels and the TES a priori CO profiles. The high CO distributions in these processed MLS maps for December 12th–19th, 2006 (top row of Fig. 2) show similar patterns to those observed by TES (mid row of Fig. 2), indicating that the enhanced CO plumes, indeed, appear in the upper troposphere away from the SE Australia fire region.

The OMI aerosol indices (AI) for December 11th–19th, 2006 are shown in Fig. 4. The large values of this parameter (*e.g.*, greater than 1) are a good indicator of the aerosol plumes generated by the biomass burning. Due to its cross track scan, OMI provides a better spatial coverage compared to TES or MLS. Although OMI's AI maps in Fig. 4 are not snap shots (*i.e.*, the orbit swath are separated by ~1.5 h), they clearly tracked the eastward propagations of at least two major fire plumes, starting on December 11th and 14th, respectively. This second event was also described in detail by Dirksen et al. (2009) using OMI data, which tracked the aerosol plumes for about 8 days.

Here, we examine the co-located TES/MLS CO observations and the OMI AI data to evaluate if the chemical tracer CO and aerosol observations on the Aura platform are consistent in describing the fire plume transport events. The coincidences of enhanced CO and AI data are only identified in a small fraction of the orbit overpasses in the region. This is due to four factors. First, TES GS observations occur every other day, and the TES and MLS footprints are along the Aura orbit tracks only. This means that there are rarely matching opportunities for the enhanced CO and AI data. Secondly, OMI AI data do not contain vertical information so that the enhanced CO VMRs observed by MLS at 215 hPa do not necessarily coincide with large OMI AI values. Third, TES DOFSs for tropospheric CO profiles in the Australia region are 1.0 to 1.4 (see Luo et al., 2007 for global values), which are not adequate to resolve the boundary layers from the upper tropospheric layers. Lastly, OMI only takes measurements in the day time. It is, therefore, hard to explain the matches or mis-matches between the high TES CO and OMI AI values. As an example, Fig. 5 shows the coincident measurements of OMI AI, MLS CO at 215 hPa, and TES CO at 681 and 215 hPa on December 16th, 2006. On this day TES had no daytime measurements to the east of 140°W and no nighttime measurements to the west of 140°W. MLS CO and OMI AI show enhancement in the same daytime orbit (circled on the plots in 30°S–50°S), while TES data are missing. In latitudes 60°S–70°S (circled), all three instruments show evidence of a fire plume. Over long distances, OMI AI could still track the fire plumes (Dirksen et al., 2009). The enhanced CO in these air parcels however, could be removed by OH in the summer.

In addition to TES and MLS observations of CO, the MOPITT and AIRS instruments on the NASA Terra and Aqua satellites also provide tropospheric CO measurements with better spatial coverage. The MOPITT CO retrievals have similar vertical sensitivities as TES (Luo et al., 2007); the AIRS CO profiles are sensitive to the mid-troposphere (McMillan et al., 2008). We examined MOPITT CO daily images

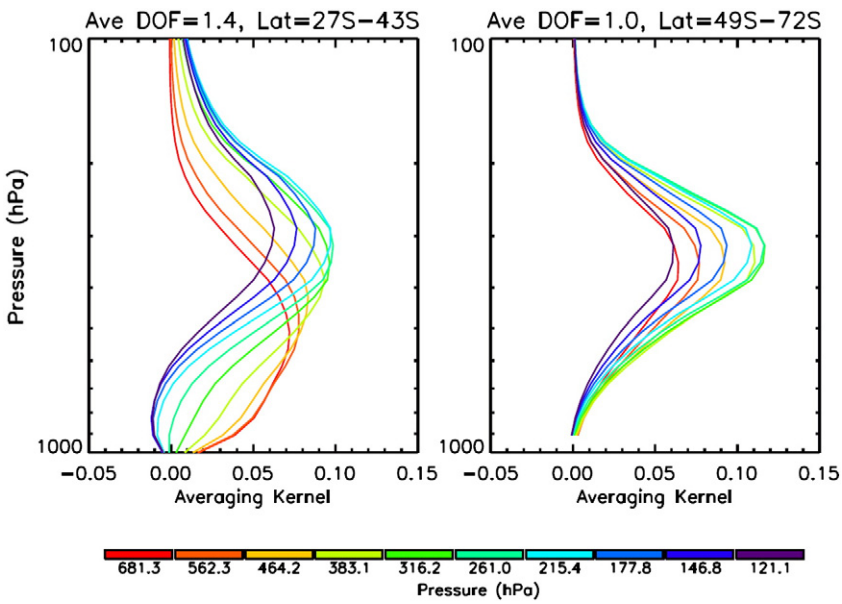

Fig. 3. Mean TES averaging kernels of selected observations, December 12th–19th, 2006. Profile selection criteria: cloudOD < 2.0, CO > 120 ppb at 215 hPa or 681 hPa. Profiles used for the left panel are in the latitude band of 27°S–43°S (number of profiles for averaging = 15). Profiles used for the right panel are in the latitude band of 49°S–72°S (number of profiles for averaging = 12).

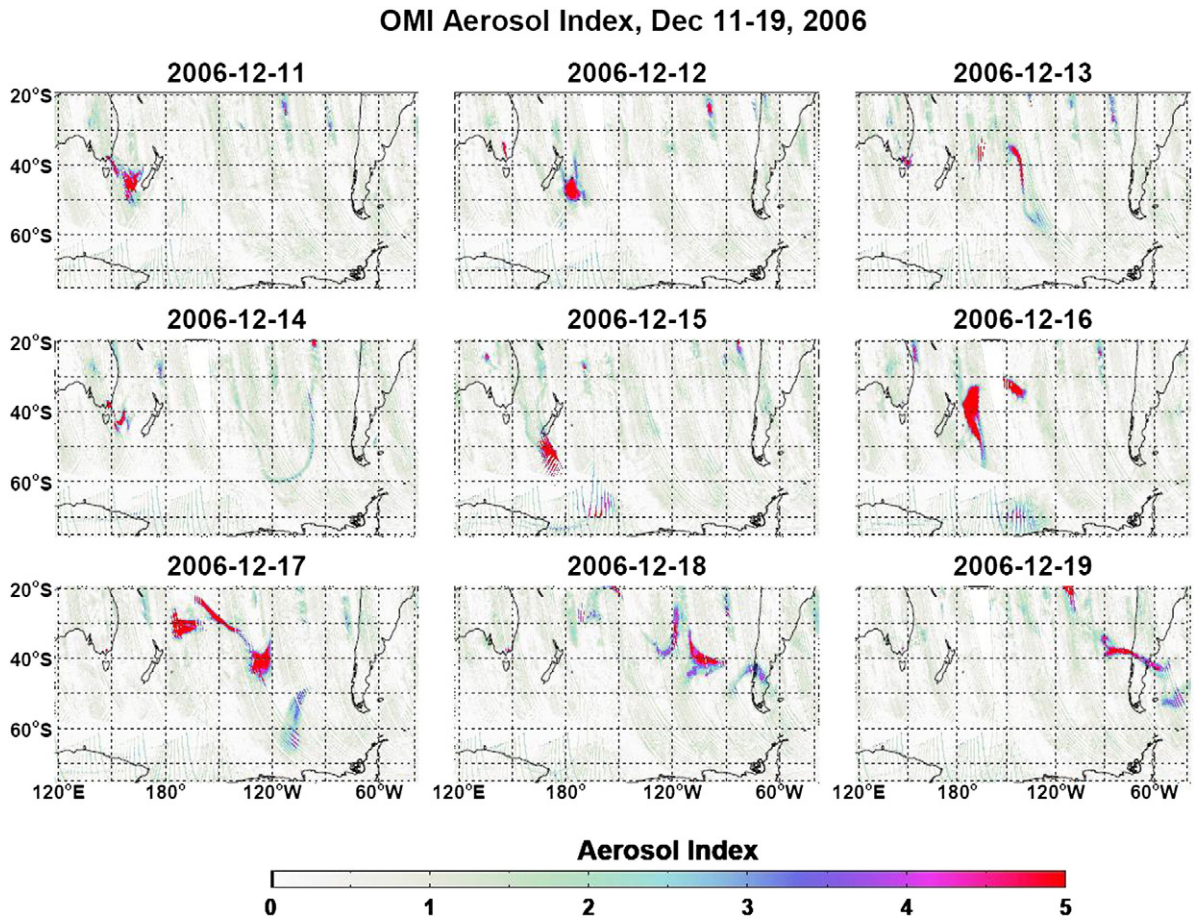

Fig. 4. OMI aerosol index (AI) in Southern Hemisphere for December 11th–19th, 2006.

(http://www.acd.ucar.edu/mopitt/MOPITT/data/plots/maps.html) and noted that MOPITT also captured enhanced CO down-wind from the SE Australia fire regions.

3. Trajectory analysis of the enhanced CO, CloudSat vertical curtains of IWC

In the previous section, we presented evidence for the long-range transport of CO from TES and MLS and AI from OMI, which originated from the known Australia fires of December, 2006. Since satellite data presented here are sparse in time and location, we ran an air parcel trajectory model to trace high CO observations backward in time to confirm their origin. The Hybrid Single Particle Lagrangian Integrated Trajectory (HYSPLIT) model developed at the Air Resources Laboratory (ARL, http://www.arl.noaa.gov/HYSPLIT_info.php) was used for this study. The meteorological data are from the Global Data Assimilation System (GDAS, http://wwwt.emc.ncep.noaa.gov/gmb/gdas/) at 3-hourly, 1 degree latitude/longitude archives at ARL.

Fig. 6 shows the air parcel trajectories starting from TES observation locations and times on December 16th–17th, 2006 for TES CO volume mixing ratios greater than 120 ppbv and 80 ppbv. Trajectories start at two TES pressure levels representing the lower and upper troposphere, 681 hPa and 215 hPa, respectively, and they are traced back 5 days and 2.5 days, respectively. MODIS 8-day fire pixels are also marked indicating the fire locations in that time period. Two conclusions can be drawn from the back trajectories shown in Fig. 6. First, the majority of TES enhanced CO air parcels at 215 hPa can be traced back to the SE Australia fire regions in about 2.5 days, which is a strong indication of the origins of the high CO values observed by TES in the upper troposphere. However, in the lower troposphere (681 hPa), the air parcels appear to originate from south of the SE Australia region, at a lower speed than those at 300–200 hPa. These trajectory analyses do not support the hypothesis that high CO observed by TES in the lower troposphere (Fig. 2 bottom panel), away from the fire areas, originated from the Australia fires. Naturally, one should place more confidence in the 2.5 day back trajectories since trajectory reliability rapidly decreases with increasing time spans. As we discussed in Section 2, these high CO observations by TES at 681 hPa are likely due to the vertical smoothing effect in the retrieval processes.

The second feature shown in Fig. 6 is that the trajectories starting at either upper or lower tropospheric levels tend to stay on their pressure levels for several days. No drastic vertical transport is displayed in these trajectories driven by the global assimilated wind fields. Vertical convections that uplift air pollutants and aerosols (*e.g.*, pyro-cumulonimbus) occurring over the fires are a possible explanation for the observed enhanced CO values that are transported far away from their source by the wind system in the upper troposphere (Fromm et al., 2005, 2006).

We examined possible supporting observations of vertical profiles of aerosols or clouds in describing this fire and transport event. The Cloud-Aerosol Lidar and Infrared Pathfinder Satellite Observation (CALIPSO) and CloudSat instruments provide vertical structures of clouds and aerosols along their orbits within NASA's A-Train constellation (http://nasascience.nasa.gov/earth-science/a-train-satellite-constellation). There was, nevertheless, a data gap in CALIPSO on December 6th–18th, 2006 (http://www.calipso.larc.nasa.gov/products/lidar/browse_images/show_calendar.php). Still, the CloudSat Ice/Liquid-Water (IWC/LWC) data were available. The CloudSat IWC/LWC were taken from the Level 2B R04 data set (Austin et al., 2009), with a horizontal resolution of 1.7 km along-track and 1.3 km cross-track, and vertical resolution

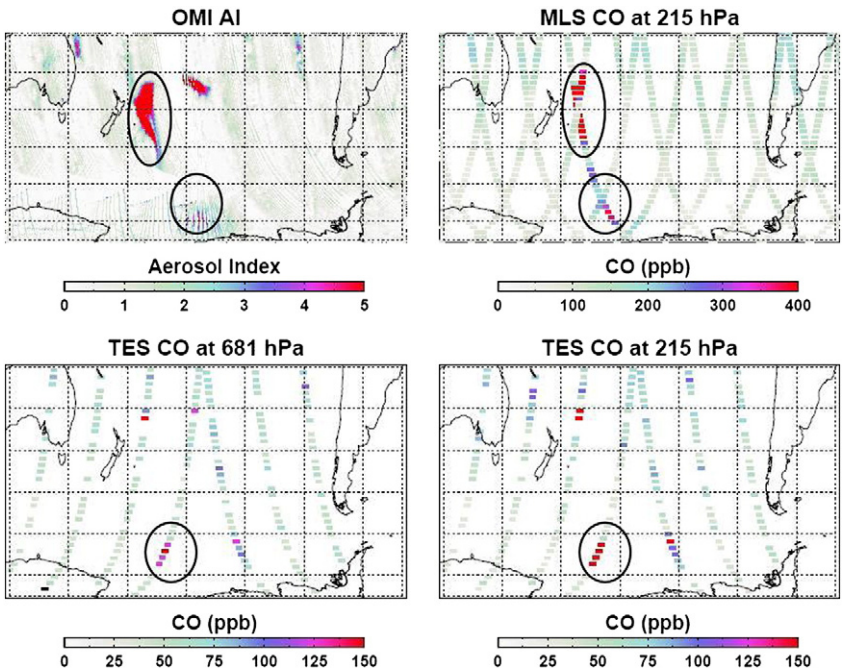

Fig. 5. Plots of OMI AI, MLS CO at 215 hPa, and TES CO at 681 hPa and 215 hPa for December 16th, 2006. Data in the circles indicates matches of enhanced AI and CO values.

of ~500 m. Since Aura is also part of the A-train (Schoeberl & Talabac, 2006) satellite constellation it follows a similar orbit, separated by less than 15 min. However, for the transport in the East–West directions, the two data sets have very few opportunities to capture the same event. Fig. 7 shows an example of backward air parcel trajectory starting from a TES location, where a high CO value was observed. We also overlaid

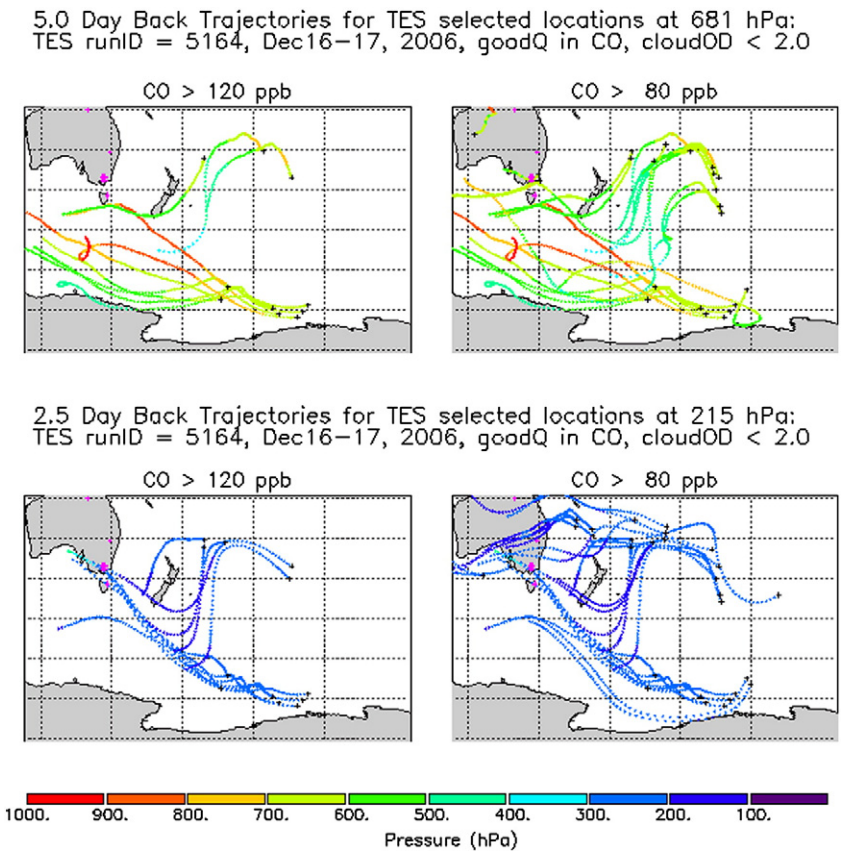

Fig. 6. Back trajectories starting at selected TES profile locations (marked by black cross symbols), December 16th–17th, 2006. Top panels are the five day trajectories starting at 681 hPa, for CO>120 ppbv (left) and CO>80 ppbv (right), respectively. Bottom panels are the 2.5 day, trajectories starting at 215 hPa, for CO>120 ppbv (left) and CO>80 ppbv (right), respectively. MODIS 8-day Climate Modeling fire pixel>50 are marked by magenta dots.

CloudSat tracks 0 to 24 h prior to the TES observation in an attempt to find coincidences between the back trajectory and the CloudSat vertical Ice-Water observations. No intersections are identified between any CloudSat orbit and the TES backward trajectories starting from all the TES high CO value locations from December 11th–19th, 2006. For this particular event, it is therefore difficult for the sparse satellite observations to comprehensively describe the process of pollutant transport.

4. GEOS-Chem model simulation of the event

Fig. 8 shows GEOS-Chem model (Bey et al., 2001) simulations of CO sampled at the TES profile footprints and times (within ±1.5 h) from December 12th–19th, 2006 in the lower troposphere (681 hPa) and in the upper troposphere (215 hPa). The model was run using GEOS-4 meteorological fields gridded to 2°×2.5° horizontal resolution and 30 vertical sigma levels up to 0.01 hPa, with output written every 3 h. Year-specific biomass burning emissions for this run were from GFEDv2 (van der Werf et al., 2006) with a temporal resolution of 8 days (based on the MODIS fire counts) but with additional CO enhancement in the Indonesian region (Nassar et al., 2009). EDGAR fossil fuel emissions of CO were used for Australia and elsewhere from the year 2000 (Olivier & Berdowski, 2001) scaled forward to 2003, as implemented by van Donkelaar et al. (2008). Not shown here are the model CO profiles with TES operators applied that simulate the TES retrieved profile assuming model CO profiles as the truth (Luo et al., 2007; Logan et al., 2008). These CO values at 681 hPa are lower than those in Fig. 8, due to the combined effects of very low CO values in the modeled upper troposphere and the TES a priori profiles.

The model simulations of CO in Fig. 8 are compared to TES observations in Fig. 2. At 681 hPa TES observed high CO concentrations over and near SE Australia on December 12–13 and 14–15, 2006. The GEOS-Chem simulations at this pressure level show similar distribution patterns of the enhanced CO. The comparisons for December 16–17 and 18–19, 2006 are not as good. This is expected since the 8-day representative emission cannot adequately describe the daily variability in the observed tracer distributions. At 215 hPa, the GEOS-Chem model showed no enhanced CO due to Australia fires as TES and MLS observations shown in Fig. 2. Nassar et al. (2009) also found an underestimate in mid-tropospheric CO relative to TES in the Indonesia and Indian Ocean region in late 2006 when GFEDv2 emissions were used directly. One probable explanation for this underestimate was the omission of the CO contribution from smoldering fires, which may not be adequately represented in GFEDv2 since it is based on MODIS observations of active fires. Nassar et al. (2009) scaled CO emissions above the GFEDv2 values for Indonesia, to account for the smoldering, which resulted in a much better spatial and temporal agreement with TES observations of elevated tropospheric CO for that region.

Although it has been shown that only 4–12% of emissions from the North American biomass fires are injected above the boundary layer (Val Martin et al., 2010), fire emission injection heights can be highly variable (Kahn et al., 2008). Therefore, another important factor indicated by the present work may be the contribution due to conditions of extreme convection with sufficient energy to efficiently transport a large amount of material from the planetary boundary layer to the UTLS — most notably referred to as pyro-cumulonimbus (pyroCb) eruptions (Fromm et al., 2005, 2006). Our GEOS-Chem simulations agree with the recent study by Jiang et al. (2008). Jiang et al. (2008) simulated UT midlatitude CO_2, using the Caltech/JPL 2-D, 3-D Geos-Chem, and 3-D Model for Ozone and Related Tracers-2 (MOZART-2) chemical transport models (CTMs), and showed that the model simulations underestimate UT CO2 when compared to aircraft data. At 215 hPa, GEOS-Chem model simulations under-predict CO concentrations from December 12th to 19th, 2006, especially from December 16th to 19th, 2006. If the high CO concentrations observed by TES and MLS from December 16th to 19th, 2006 are due to pyroCbs, then the lack of congruence between GEOS-Chem simulations and TES/MLS observations (*i.e.*, the drastic underestimation of CO by GEOS-Chem at 215 hPa) is not surprising as GEOS-Chem does not presently account for pyroCbs. Despite a slight underestimation, GEOS-Chem simulates TES CO observations well from December 12th to 17th, 2006, but overestimates the amount of CO over SE Australia and underestimates the amount of CO transported SE of Australia from December 18th to 19th, 2006.

Dirksen et al. (2009) used the TM4 chemistry transport model, constrained by OMI O_2–O_2 and AAI retrievals, to investigate the height and subsequent transport of the biomass burning plume during the December Australian forest fires, by releasing a passive, but water soluble, tracer in TM4. They conducted simulations with tracer emissions at the surface level (1013 hPa) and at 540 hPa, which resulted in similar tracer vertical distributions with highest tracer concentrations between 300 and 400 hPa. This result suggests that TM4 can, to some degree, simulate the lofting of the plume by the cold front, but also that the model fails to push the plume towards altitudes where it is picked up by the jet stream and where it is actually observed. To better simulate

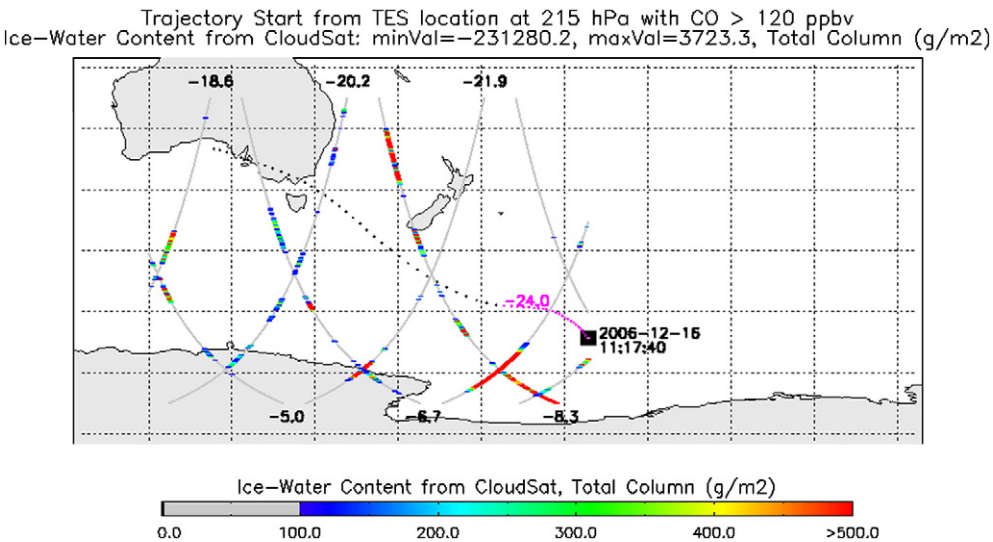

Fig. 7. A backward trajectory started from a TES profile location (dark square). The trajectory is represented by the black dotted curve, and the overlaid magenta curve represents the trajectory portion of 0 to −24 h. The light-gray tracks indicate the location of the CloudSat orbits with colored ice-water content total column measurements. The CloudSat overpass times relative to the TES observation times (or zero hour) are in black for the corresponding orbit tracks (0 to −24 h orbits).

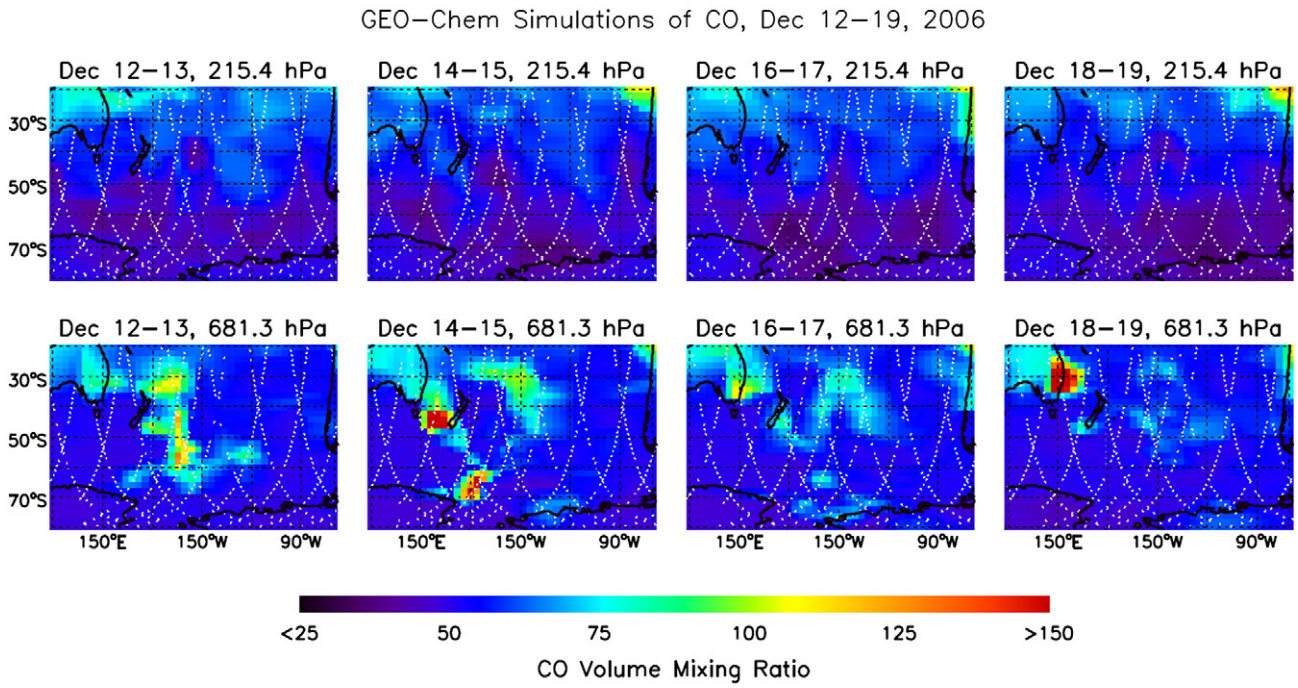

Fig. 8. GEOS-Chem simulations of CO sampled at the TES profile footprints and times, December 12th–19th, 2006. Top row: GEOS-Chem CO at 215 hPa; Bottom row: GEOS-Chem CO at 681 hPa. The four columns: TES Global Surveys of December 12th–13th, 14th–15th, 16th–17th, and 18th–19th, 2006.

the effects of pyro-convection, Dirksen et al. (2009) released the tracer at 248 hPa, which resulted in tracer plumes that are higher by 2–5 km and closer to the observed CALIOP plume altitudes. Extreme lofting by pyro-convection, although rare, is important because of the rapid pathway it offers for biomass combustion products to reach the upper troposphere or lower stratosphere (Fromm et al., 2005). Similar to GEOS-Chem, the TM4 model does not incorporate pyroCbs. Most CTMs do not treat lofting of fire plumes properly, and the common way to do so in such models studying forest fire events is to impose an injection height as Dirksen et al. (2009) did in their study. The injection height of emission plumes varies considerably amongst fires, and the lofting of fire emissions depends on the energy of the fire and the local meteorological conditions (Hyer et al., 2007). Therefore, an appropriate parameterization of the lofting is needed, which should account for vegetation type to estimate the heat flux and information on the fire size to calculate the buoyancy flux (Freitas et al., 2007). A 1-D plume-rise model, adapted from Freitas et al. (2007), is currently being developed to be implemented in GEOS-Chem (Dirksen et al., 2009).

5. Conclusions

In this paper, we present Aura satellite observations of chemical tracer CO (TES and MLS instruments) and aerosol indices (OMI instrument) in regions down-wind from the Australian fires of December 2006. We also examined the tracer pathways via the HYSLPLIT trajectory model, powered by GDAS wind fields, which trace the enhanced CO air parcels back to the known fire sources in the upper troposphere. The trajectories stayed on the upper tropospheric pressure level for 2–3 days between the fire origins and the observation locations. These observations and analyses suggest that for this particular event, the fire generated tracer CO and aerosols in the smoke were uplifted to the mid-upper-troposphere at the fire sources possibly via the pyro-convection mechanism suggested previously (Fromm et al., 2005, 2006) and carried away by the strong horizontal wind system in the upper troposphere.

The TES retrievals of CO enhancements in the lower troposphere can be traced back to the general area to the south of the fire origins with slower air movement compared to the upper troposphere. We examined the vertical information in the TES CO profile retrievals. The DOFS are 1.4 and 1.0 for those TES CO profiles between 27°S to 43°S and 49°S to 72°S, respectively. The TES averaging kernels, which describe the contributions of the true CO profile to the retrieved value, at each pressure level, peak around 300 hPa. TES reported high CO values in the lower troposphere away from where the fire sources are, therefore, partially due to the enhancement in CO in the mid-upper troposphere.

GEOS-Chem model simulations of tropospheric CO, using GFEDv2 biomass burning emissions, are examined by extracting model data along TES observation footprints and times. Without the mechanisms (*e.g.*, pyroCb) that strongly uplift the fire produced CO and aerosols into the upper troposphere, no CO enhancements in model simulations are shown in the upper troposphere compared to the background values. Model CO fields in the lower troposphere do show the production and the transport of high CO values at and away from the fire source. These CO concentrations are in qualitative agreement with TES observations from December 12th and 15th, 2006.

TES, MLS, and OMI observations of concentrations of the chemical tracer, CO, and the vertical aerosol loadings together with the meteorological wind fields provide evidence for transport pathways of pollutants produced in the December 2006 Australian fires. However, the observations are too sparse and limited in time, which does not allow for a definitive description of the time evolution of the entire event. The inadequate vertical resolution in the TES CO profiles does not allow us to distinguish the CO in the boundary layer from the mid/upper troposphere. Although other A-train data (*e.g.*, vertical versus orbit track curtains of CloudSat ice-water content) provide complementary information, it is difficult to correlate to the same transport event as observed with the Aura data. The new generation of satellite instruments for tropospheric chemistry, *e.g.*, on a geo-stationery platform (ref), should provide improved vertical resolution of tracer profiles, better spatial and temporal coverage, and opportunities to capture the convection moments via their IR or Vis/UV spectra in the small pix-footprints defined for urban air pollution events. Future GEOS-Chem simulations are needed to validate this conjecture as the PyroCb mechanism is currently not incorporated in GEOS-Chem.

Acknowledgements

We would like to thank the helpful discussions on this work with Drs. Jennifer Logan, Jimmie Lopez, Line Jourdain, Lenny Pfister and O. Torres. J. H. Jiang acknowledges the support from the NASA ACMAP program. The research described in this paper was carried out at the Jet Propulsion Laboratory, California Institute of Technology, under a contract with the National Aeronautics and Space Administration. Funding at the University of Toronto was provided by the Natural Sciences and Engineering Research Council (NSERC) of Canada.

References

Andrea, M., & Merlet, P. (2001). Emissions of trace gases and aerosols from biomass burning. *Global Biogeochemical Cycles*, *15*, 955—966.

Arino, O., Plummer, S., & Casadio, S. (2007). Fire disturbance: The twelve year time series of the ATSR World Fire Atlas. *Proceedings of the ENVISAT symposium 2007, SP-636*, ESA.

Austin, R. T., Heymsfield, A. J., & Stephens, G. L. (2009). Retrieval of ice cloud microphysical parameters using the CloudSat millimeter-wave radar and temperature. *Journal of Geophysical Research*, *114*, D00A23, doi:10.1029/2008JD010049.

Badr, O., & Probert, S. D. (1994). Carbon monoxide concentration in the earth's atmosphere. *Applied Energy*, *49*, 99—143.

Bakwin, P. S., Tans, P. P., & Novelli, P. C. (1994). Carbon monoxide budget in the Northern Hemisphere. *Geophysical Research Letters*, *21*, 433—436.

Beer, R. (2006). TES on the Aura mission: Scientific objectives, measurements, and analysis overview. *IEEE Transactions on Geoscience and Remote Sensing*, *44*, 1102—1105.

Bey, I., Jacob, D. J., Yantosca, R. M., Logan, J. A., Field, B. D., Fiore, A. M., et al. (2001). Global modeling of tropospheric chemistry with assimilated meteorology: Model description and evaluation. *Journal of Geophysical Research*, *106*, 23,073—23,089.

Cowling, R. M., & Lamont, B. B. (1985). Variation in serotiny of three *Banksia* species along a climatic gradient. *Austral Ecology*, *10*, 345—350.

Crutzen, P., & Andrea, M. (1990). Biomass burning in the tropics: Impact on atmospheric chemistry and biogeochemical cycles. *Science*, *250*, 1669—1678.

Dirksen, R. J., Boersma, K. F., Laat, J. d., Stammes, P., van der Werf, G. R., Martin, M. V., et al. (2009). An aerosol boomerang: Rapid around-the-world transport of smoke from the December 2006 Australian forest fires observed from space. *Journal of Geophysical Research*, *114*, doi:10.1029/2009JD012360.

Duncan, B. N., Logan, J. A., Bey, I., Megretskaia, I. A., Yantosca, R. M., Novelli, P. C., et al. (2007). Global budget of CO, 1988–1997: Source estimates and validation with a global model. *Journal of Geophysical Research*, *112*, D22301, doi:10.1029/2007JD009459.

Edwards, D. P., Emmons, L. K., Hauglustaine, D. A., Chu, D. A., Gille, J. C., Kaufman, Y. J., et al. (2004). Observations of carbon monoxide and aerosols from the Terra satellite: Northern Hemisphere variability. *Journal of Geophysical Research*, *109*, D24202, doi:10.1029/2004JD004727.

Freitas, S. R., Longo, M., Chatfield, R., Latham, D., Silva Dias, M. A. F., Andreae, M. O., et al. (2007). Including the sub-grid scale plume rise of vegetation fires in low resolution atmospheric transport models. *Atmospheric Chemistry and Physics*, *7*, 3385—3398.

Fromm, M., Bevilacqua, R., Servanckx, R., Rosen, J., Thayer, J. P., Herman, J., et al. (2005). Pyro-cumulonimbus injection of smoke to the stratosphere: Observations and impact of a super blowup in northwestern Canada on 3–4 August 1998. *Journal of Geophysical Research*, *110*, D08205, doi:10.1029/2004JD005350.

Fromm, M., Tupper, A., Rosenfeld, D., Servranckx, R., & McRae, R. (2006). Violent pyro-convective storm devastates Australia's capital and pollutes the stratosphere. *Geophysical Research Letters*, *33*, L05815, doi:10.1029/2005GL025161.

Guan, H., Chatfield, R. B., Freitas, S. R., Bergstrom, R. W., & Longo, K. M. (2008). Modeling the effect of plume-rise on the transport of carbon monoxide over Africa with NCAR CAM. *Atmospheric Chemistry and Physics*, *8*, 6801—6812.

Hyer, E. J., Allen, D. J., & Kasischke, E. S. (2007). Examining injection properties of boreal forest fires using surface and satellite measurements of CO transport. *Journal of Geophysical Research*, *112*, D18307, doi:10.1029/2006JD008232.

Jiang, X., Li, Q., Liang, M. C., Shia, R. -L., Chahine, M. T., Olsen, E. T., et al. (2008). Simulation of upper tropospheric CO_2 from chemistry and transport models. *Global Biogeochemical Cycles*, *22*, GB4025, doi:10.1029/2007GB003049.

Justice, C. O., Giglio, L., Korontzi, S., Owens, J., Morisette, J., Roy, D., et al. (2002). The MODIS fire products. *Remote Sensing of Environment*, *83*, 244—262.

Kahn, R. A., Chen, Y., Nelson, D. L., Leung, F. -Y., Li, Q., Diner, D. J., et al. (2008). 1 Wildfire smoke injection heights: Two perspectives from space. *Geophysical Research Letters*, *35*, L04809, doi:10.1029/2007GL032165.

Kasischke, E. S., & Tretsky, M. R. (2007). Recent changes in the fire regime across the North American boreal region — Spatial and temporal patterns of burning across Canada and Alaska. *Geophysical Research Letters*, *33*, L09703, doi:10.1029/2006GL025677.

Khalil, M. A. K., & Rasmussen, R. A. (1988). Carbon monoxide in the earth's atmosphere: Indications of a global increase. *Nature*, *332*, 242—245.

Khalil, M. A. K., & Rasmussen, R. A. (1994). Global decrease in atmospheric carbon monoxide concentration. *Nature*, *370*, 639—641.

Lamarque, J. -F., Edwards, D. P., Emmons, L. K., Gille, J. C., Wilhelmi, O., Gerbig, C., et al. (2003). Identification of CO plumes from MOPIT data: Application to the August 2000 Idaho Montana forest fires. *Geophysical Research Letters*, *30*, 1688, doi:10.1029/2003GL017503.

Lapina, K., Honrath, R. E., Owen, R. C., ValMartin, M., & Pfister, G. (2006). Evidence of significant large-scale impacts of boreal fires on ozone levels in midlatitude Northern Hemisphere free troposphere. *Geophysical Research Letters*, *33*, L10815, doi:10.1029/2006GL025878.

Liousse, C., Penner, J. E., Chuang, C., Walton, J. J., Edleman, H., & Cachier, H. (1996). A global three-dimensional model study of carbonaceous aerosols. *Journal of Geophysical Research*, *101*, 19411—19432.

Livesey, N. J., Fromm, M. D., Waters, J. W., Manney, G. L., Santee, M. L., & Read, W. G. (2004). Enhancements in lower stratospheric CH_3CN observed by UARS MLS fillowing boreal forest fires. *Journal of Geophysical Research*, *109*, D06308, doi:10.1029/2003JD004055.

Livesey, N. J., Filipiak, M. J., Froidevaux, L., Read, W. G., Lambert, A., Santee, M. L., et al. (2008). Validation of Aura Microwave Limb Sounder O_3 and CO observations in the upper troposphere and lower stratosphere. *Journal of Geophysical Research*, *113*, D15S02, doi:10.1029/2007JD008805.

Logan, J. A., Prather, J. M., Wofsy, S. C., & McElroy, M. B. (1981). Tropospheric chemistry: A global perspective. *Journal of Geophysical Research*, *86*, 710—7254.

Logan, J. A., Megretskaia, I. A., Nassar, R., Murray, L. T., Zhang, L., Bowman, K. W., et al. (2008). Effects of the 2006 El Niño on tropospheric composition as revealed by data from the Tropospheric Emission Spectrometer (TES). *Geophysical Research Letters*, *35*, L03816, doi:10.1029/2007GL031698.

Luo, M., Rinsland, C. P., Rodgers, C. D., Logan, J. A., Worden, H., Kulawik, S., et al. (2007). Comparison of carbon monoxide measurements by TES and MOPITT: Influence of a priori data and instrument characteristics on nadir atmospheric species retrievals. *Journal of Geophysical Research*, *112*, D09303, doi:10.1029/2006JD007663.

McMillan, W. W., Warner, J. X., McCourt Comer, M., Maddy, E., Chu, A., Sparling, L., et al. (2008). AIRS views transport from 12 to 22 July 2004 Alaskan/Canadian fires: Correlation of AIRS CO and MODIS AOD with forward trajectories and comparison of AIRS CO retrievals with DC-8 in situ measurements during INTEX-A/ICARTT. *Journal of Geophysical Research*, *113*, D20301, doi:10.1029/2007JD009711.

Nassar, R., Logan, J. A., Megretskaia, I. A., Murray, L. T., Zhang, L., & Jones, D. B. A. (2009). Analysis of tropospheric ozone, carbon monoxide and water vapor during the 2006 El Nino using TES observations and the GEOS-Chem model. *Journal of Geophysical Research*, *114*, D17304, doi:10.1029/2009JD011760.

Nedelec, P., Thouret, V., Brioude, J., Sauvage, B., Cammas, J. -P., & Stohl, A. (2005). Extreme CO concentrations in the upper troposphere over northeast Asia in June 2003 from the in situ MOZAIC aircraft data. *Geophysical Research Letters*, *32*, L14807, doi:10.1029/2005GL023141.

Novelli, P. C., Masarie, K. A., Tans, P. P., & Lang, P. M. (1994). Recent changes in atmospheric carbon monoxide. *Science*, *263*, 1587—1590.

Olivier, J. G. J., & Berdowski, J. J. M. (2001). Global emissions sources and sinks in: Climate system. In J. Berdowski, R. Guicherit, & B. J. Heij (Eds.), Lisse, The Netherlands: A.A. Balkema Publishers/Swets & Zeitlinger Publishers90 5809 255 0.

Osterman, G., et al. (2009). *TES level 2 data user's guide*. http://eosweb.larc.nasa.gov/PRODOCS/tes/UsersGuide/TES_L2_Data_Users_Guide.pdf.

Parrish, D. D., Trainer, M., Hereid, D., Williams, E. J., Olszyna, K. J., Harley, R. A., et al. (2002). Decadal change in carbon monoxide to nitrogen oxide ratio in U.S. vehicular emissions. *Journal of Geophysical Research*, *107*, 4140, doi:10.1029/2001JD000720.

Rodgers, C. D. (2000). Inverse methods for atmospheric sounding: Theory and practice. Hackensack, N. J.: World Sci.

Salvatore, R., Moya, D., Pulido, L., Lovreglio, R., Lopez-Serrano, R. R., Heras, J. D. L., et al. (2010). Morphological and anatomical differences in Aleppo pine seeds from serotinous and non-serotinous cones. *New Forests*, *39*, 329—341.

Seiler, W., & Crutzen, P. J. (1980). Estimates of gross and net fluxes of carbon between the biosphere and the atmosphere from biomass burning. *Climatic Change*, *2*, 207—247.

Schoeberl, M. R., & Talabac, S. (2006). The Sensor Web: A future technique for science return. In G. Visconti (Ed.), *Observing systems for atmospheric composition* (pp. 203—206). New York: Springer.

Torres, O., Tanskanen, A., Veihelmann, B., Ahn, C., Braak, R., Bhartia, P. K., et al. (2007). Aerosols and surface UV products from Ozone Monitoring Instrument observations: An overview. *Journal of Geophysical Research*, *112*, D24S47, doi:10.1029/2007JD008809.

Turquety, S., Logan, J. A., Jacob, D. J., Hudman, R. C., Leung, F. -Y., Heald, C. L., et al. (2007). Inventory of boreal fire emissions for North America in 2004: Importance of peat burning and pyroconvective injection. *Journal of Geophysical Research*, *112*, D12S03, doi:10.1029/2006JD007281.

Val Martin, M., Logan, J. A., Kahn, R. A., Leung, F. -Y., Nelson, D. L., & Diner, D. J. (2010). Smoke injection heights from fires in North America: Analysis of 5 years of satellite observations. *Atmospheric Chemistry and Physics*, *10*, 1491—1510.

van der Werf, G. R., Randerson, J. T., Giglio, L., Collatz, G. J., Kasibhatla, P. S., & Arellano, A. F., Jr. (2006). Interannual variability in global biomass burning emissions from 1997 to 2004. *Atmospheric Chemistry and Physics*, *6*, 3423—3441.

van der Werf, G. R., Randerson, J., Giglio, L., Gobron, N., & Dolman, H. (2008). Climate controls on the variability of fires in the tropics and subtropics. *Global Biogeochemical Cycles*, *22*, GB3028, doi:10.1029/2007GB003122.

van Donkelaar, A., Martin, R. V., Leaitch, W. R., Macdonald, A. M., Walker, T. W., Streets, D. G., et al. (2008). Analysis of aircraft and satellite measurements from the Intercontinental Chemical Transport Experiment (INTEX-B) to quantify long-range transport of East Asian sulfur to Canada. *Atmospheric Chemistry and Physics*, *8*, 2999—3014.

Waters, J. W., Froidevaux, L., Harwood, R. S., Jarnot, R. F., Pickett, H. M., Read, W. G., et al. (2006). The Earth Observing System Microwave Limb Sounder (EOS MLS) on the Aura satellite. *IEEE Transactions on Geoscience and Remote Sensing*, *44*(5), 1075—1092.

West, J. J., Naik, V., Horowitz, L., & Fiore, A. M. (2009a). Effect of regional precursor emission controls on long-range ozone transport — Part 1: Short-term changes in ozone air quality. *Atmospheric Chemistry and Physics*, *9*, 6077—6093.

West, J. J., Naik, V., Horowitz, L., & Fiore, A. M. (2009b). Effect of regional precursor emission controls on long-range ozone transport — Part 2: Steady-state changes in ozone air quality and impacts on human mortality. *Atmospheric Chemistry and Physics*, *9*, 6095—6107.

Yurganov, L. N., McMillan, W. W., Dzhola, A. V., Grechko, E. I., Jones, N. B., & van der Werf, G. (2008). Global AIRS and MOPITT CO measurements: Validate, comparison, and links to biomass burning variations and carbon cycle. *Journal of Geophysical Research*, *113*, D09301, doi:10.1029/2007JD009229.

Yurganov, L. N., Grechko, E. I., & Dzhola, A. V. (1997). Variations in carbon monoxide density in the total atmospheric column over Russia between 1970 and 1995: Upward trend and disturbances attributed to the influence of volcanic aerosols and forest fires. *Geophysical Research Letters*, *24*, 1231—1234.

Yurganov, L. N., Blumenstock, T., Grechko, E. I., Hase, F., Hyer, E. J., Kasischke, E. S., et al. (2004). A quantitative assessment of the 1998 carbon monoxide emission anomaly in the Northern Hemisphere based on total column and surface concentration measurements. *Journal of Geophysical Research*, *109*, D15305, doi:10.1029/2004JD004559.